

High-temperature in situ crystallographic observation of reversible gas sorption in impermeable organic cages

Seung Bin Baek^{a,1}, Dohyun Moon^{b,1}, Robert Graf^c, Woo Jong Cho^a, Sung Woo Park^d, Tae-Ung Yoon^e, Seung Joo Cho^f, In-Chul Hwang^{d,2}, Youn-Sang Bae^e, Hans W. Spiess^c, Hee Cheon Lee^d, and Kwang S. Kim^{a,3}

^aDepartment of Chemistry and Center for Superfunctional Materials, Ulsan National Institute of Science and Technology, Ulsan 689-798, Korea; ^bPohang Accelerator Laboratory, Pohang 790-834, Korea; ^cMax-Planck-Institute for Polymer Research, 55128, Mainz, Germany; ^dDepartment of Chemistry, Pohang University of Science and Technology, Pohang 790-784, Korea; ^eDepartment of Chemical and Biomolecular Engineering, Yonsei University, Seoul 120-749, Korea; and ^fDepartment of Cellular Molecular Medicine, College of Medicine, Chosun University, Gwangju 501-759, Korea

Edited by Galen D. Stucky, University of California, Santa Barbara, CA, and approved October 7, 2015 (received for review March 6, 2015)

Crystallographic observation of adsorbed gas molecules is a highly difficult task due to their rapid motion. Here, we report the in situ single-crystal and synchrotron powder X-ray observations of reversible CO₂ sorption processes in an apparently nonporous organic crystal under varying pressures at high temperatures. The host material is formed by hydrogen bond network between 1,3,5-tris-(4-carboxyphenyl)benzene (H₃BTB) and *N,N*-dimethylformamide (DMF) and by π - π stacking between the H₃BTB moieties. The material can be viewed as a well-ordered array of cages, which are tight packed with each other so that the cages are inaccessible from outside. Thus, the host is practically nonporous. Despite the absence of permanent pathways connecting the empty cages, they are permeable to CO₂ at high temperatures due to thermally activated molecular gating, and the weakly confined CO₂ molecules in the cages allow direct detection by in situ single-crystal X-ray diffraction at 323 K. Variable-temperature in situ synchrotron powder X-ray diffraction studies also show that the CO₂ sorption is reversible and driven by temperature increase. Solid-state magic angle spinning NMR defines the interactions of CO₂ with the organic framework and dynamic motion of CO₂ in cages. The reversible sorption is attributed to the dynamic motion of the DMF molecules combined with the axial motions/angular fluctuations of CO₂ (a series of transient opening/closing of compartments enabling CO₂ molecule passage), as revealed from NMR and simulations. This temperature-driven transient molecular gating can store gaseous molecules in ordered arrays toward unique collective properties and release them for ready use.

in situ X-ray diffraction | nonporous organic crystalline material | CO₂ sorption

Guest capture, storage, and removal in porous materials have been interesting topics in chemistry (1–7). The porosity of solids is one of the important factors determining their potential applications in guest storage. Because the storage generally uses void spaces interconnected through large open channels between the voids inside the crystal, nonporous or seemingly nonporous materials have received less attention. Over the past decades, nevertheless, due to the potential for selective guest capture and release in a controlled manner there have been attempts to study such materials which include calixarenes (8–17), 4-phenoxyphenol (18), biconcave molecules (19), tris(5-acetyl-3-thienyl)methane (20), metallocyclic complex (21), clarithromycin (22), and metal-organic frameworks (23, 24).

Single-crystal X-ray diffraction can provide the crucial information on the binding interactions or structural changes of guest molecules within pores (25–27). However, the crystallographic observation of adsorbed gas adsorbents generally has not been possible due to the poor crystalline order of adsorbents upon removing residual solvent/guest molecules and the high mobility of gases even at low temperatures. Only a limited number of gas-adsorbed

single-crystal structures have been determined at low temperatures (16, 28–36).

If the permanent channels large enough for the guest diffusion between voids are not present, such a material is nonporous and impermeable to the guest molecules even if there are cages available for the guest storage. If transient pathways between voids can be made with molecular gates in special conditions, the cages can be used for storing special molecules in well-ordered arrays. Furthermore, if they confine the gas molecules in cages, it would be possible to observe the gas molecule using single-crystal X-ray crystallography at high temperatures, even for the relatively weak interactions between the frameworks and gas molecules. Based on this assumption, we studied the reversible CO₂ sorption in a seemingly nonporous organic crystalline cage material composed of 1,3,5-tris-(4-carboxyphenyl)benzene (H₃BTB) and *N,N*-dimethylformamide (DMF) using in situ single-crystal and synchrotron powder X-ray diffraction at 323 K. The dynamical motion of CO₂ is investigated using solid-state NMR as well as density functional calculations of transition pathways and molecular dynamics (MD) simulations.

Significance

Crystallographic observation of adsorbed gas molecules at high temperatures is a highly challenging task due to their rapid motion. We provide evidence of restrained motions in a self-assembled organic crystal with small isolated cages, inside which the confined CO₂ molecules can be identified with in situ X-ray diffraction technique at the high temperature. Although the crystal is nonporous, the CO₂ molecules can permeate into the crystal because of thermally activated transient pathways between the cages. We show that the flexible nature of the transient pathways leads to the temperature-driven reversible CO₂ sorption, understanding of which can contribute to the design of a system with controlled capture/release of gas molecules.

Author contributions: S.B.B. and K.S.K. designed research; S.B.B., D.M., R.G., W.J.C., S.W.P., T.-U.Y., S.J.C., I.-C.H., H.W.S., and H.C.L. performed research; S.B.B., D.M., R.G., W.J.C., S.W.P., I.-C.H., Y.-S.B., H.W.S., and H.C.L. analyzed data; and S.B.B., W.J.C., H.W.S., and K.S.K. wrote the paper.

The authors declare no conflict of interest.

This article is a PNAS Direct Submission.

Freely available online through the PNAS open access option.

Data deposition: The atomic coordinates and structure factors have been deposited in the Cambridge Crystallographic Data Centre, www.ccdc.cam.ac.uk (reference nos. CCDC-1008184, CCDC-1008185, and CCDC-1008186).

¹S.B.B. and D.M. contributed equally to this work.

²Present address: Center for Nanomaterials/Korea Center for Artificial Photosynthesis, Sogang University, Seoul 121-854, Korea.

³To whom correspondence should be addressed. Email: kimks@unist.ac.kr.

This article contains supporting information online at www.pnas.org/lookup/suppl/doi:10.1073/pnas.1504586112/-DCSupplemental.

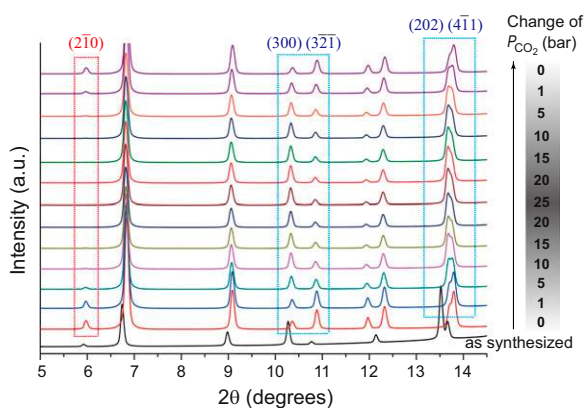


Fig. 2. In situ synchrotron PXRD patterns under varying pressures of CO₂ at 323 K. The red dotted square represents the changes in diffraction peaks at the (2-1 0) plane accompanying CO₂ adsorption and desorption. The blue dotted squares represent the intensity changes in diffraction peaks accompanying framework expansions and contractions upon reversible CO₂ sorption.

for CO₂, N₂, O₂, and CH₄ at 323 K. Among them, CO₂ shows the highest gas adsorption capacity (*SI Appendix, Fig. S7*). The selective sorption of CO₂ from the gas mixture is essential in CO₂ capture applications. All equilibrium adsorption isotherms are well-fitted to either single-site Langmuir or single-site Langmuir–Freundlich isotherm model, yielding the fitting parameters for the CO₂, N₂, O₂, and CH₄ (*SI Appendix, Fig. S8*). With these parameters, we then estimated the equilibrium selectivities for CO₂ over N₂, CH₄, and O₂. We used ideal adsorbed solution theory (IAST) (39, 40) to predict the behavior of binary (50:50) gas mixture in the pressure ranges of 1–15 bar. For a CO₂/N₂ binary mixture, IAST selectivity values were calculated to be 17 (at 1 bar) and 13 (at 15 bar). The IAST selectivity values for a CO₂/O₂ mixture were estimated to be 16 (at 1 bar) and 8 (at 15 bar). The most striking selectivity values were estimated for a CO₂/CH₄ mixture, where the selectivity increases rapidly from 12 (at 1 bar) to ~492 (at 15 bar) (*SI Appendix, Table S3 and Fig. S9*). Both quadrupole moments and polarizability of gases should be taken into account to explain the high selectivity of CO₂ over other gases. The larger quadrupole moment (13.4×10^{-40} C·m²) and polarizability (26.5×10^{-25} cm³) of CO₂ compared with those of CH₄ (no quadrupole moment, 26.0×10^{-25} cm³), N₂ (4.7×10^{-40} C·m², 17.6×10^{-25} cm³), and O₂ (1.3×10^{-40} C·m², 16.0×10^{-25} cm³) (41) leads to a higher affinity to the surface of the crystal. Furthermore, because its kinetic diameter (3.30 Å) is the smallest among the tested gases (CH₄, 3.82 Å; N₂, 3.64 Å; O₂, 3.46 Å), it is the easiest for CO₂ to penetrate into the inner cage. The kinetic diameter difference also explains the large enhancement of the selectivity for CO₂ over CH₄ at high pressures, along with the difference in polarity. To experimentally confirm the selective separation of CO₂ from gas mixtures as expected from IAST analysis, we carried out breakthrough experiments with binary gas mixtures of CO₂/CH₄ (50/50) and CO₂/N₂ (15/85) at 323 K and 1 bar (*SI Appendix, Fig. S10*). Unlike the IAST analysis, the breakthrough curve for the CO₂/CH₄ mixture shows no selectivity of CO₂ over CH₄. The CO₂/N₂ mixture shows poor selectivity only in the very early stage of the breakthrough measurement. The differences in calculated and experimental selectivities are likely to be due to slow kinetics of the intraparticle diffusion of the gas molecules. The adsorption rate analysis revealed that the CO₂ adsorption on **apo-1** is a very slow process with an activation energy of 10.1 kcal/mol (*SI Appendix, Table S4 and Fig. S11*). Thus, only the interparticle diffusion and surface adsorption/desorption are responsible for the observed selectivity. The difference in diffusion rate is negligible for CO₂ and CH₄, whereas a small difference for

CO₂ and N₂ can be noticed from the short time delay before the CO₂ diffuses out of the sample.

To gain better insights into the interactions of adsorbed CO₂ molecule with the framework, we performed solid-state magic angle spinning (MAS) NMR experiments (42, 43). ¹H-¹³C heteronuclear correlation experiments (44–46) of **apo-1** and **1-CO₂** provided insight into structural changes upon the adsorption of CO₂ molecules. The signal of CO₂ molecules observed at 123 ppm in **1-CO₂** correlates strongly with one of the DMF methyl signal (Fig. 3). The two methyl groups of DMF are inequivalent and exhibit two distinct NMR signals at room temperature. The ¹H signal correlating to the ¹³C CO₂ signal is assigned to the methyl group in the *cis* position to the DMF-CO double bond. Additionally, there are two weaker correlation signals of the adsorbed CO₂ molecules. The first correlates to the *ortho* ¹H sites of the outer phenyl rings of H₃BTB, and the second correlates to the DMF methyl group in the *trans* position, which originates from molecular fluctuation of the CO₂ and DMF molecules in **1-CO₂**. This indicates that the CO₂ molecules are located most likely between the DMF molecules and the outer phenyl rings of H₃BTB. This is consistent with our density functional tight binding (DFTB) method (47, 48)-based MD simulations, where the CO₂ carbon atom spends most of its time near the *cis* CH₃ group. From a series of MD simulations, we calculated the distances between the carbon atom of CO₂ and various types of hydrogen atoms. Upon analyzing trajectory, the CO₂ molecule on average lies at the center of the cage, which is consistent with the X-ray structure. However, the average of horizontal (i.e., parallel to the H₃BTB units) displacement with respect to the cage center is 1.01 Å, and the SD is 0.50 Å, meaning that the CO₂ molecule is deviated from the cage center. A more detailed analysis reveals that the carbon atom spends 96% of its time near (<3.5 Å) the *cis*-CH₃, 17% near the *ortho*-CH, and 15% near the *trans*-CH₃. The percentages sum up to more than 100% because the interaction sites are not mutually exclusive. Because the *cis*-CH₃ groups are directed inward, the CO₂ molecule can be close to *cis*-CH₃ and at the same time interact with other protons as well (*SI Appendix*, Fig. S12). The vertical (i.e., perpendicular to the H₃BTB units) fluctuation of

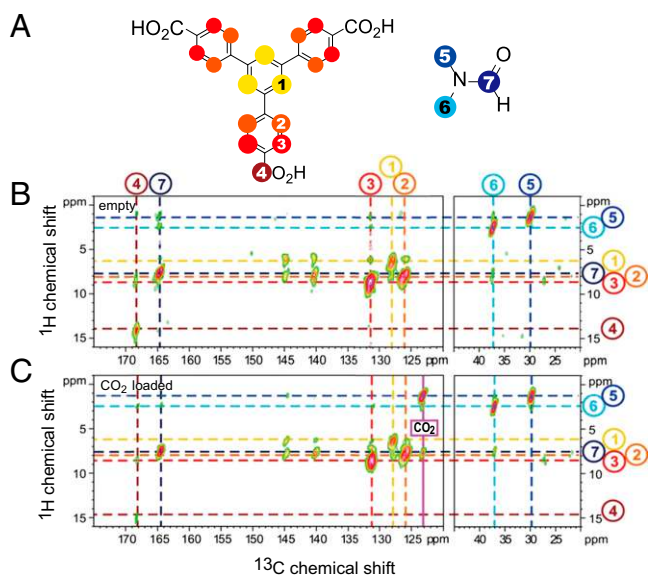


Fig. 3. Solid-state ^1H - ^{13}C heteronuclear correlation spectra. (A) Molecular precursors with the color code for spectral assignment of NMR signals. (B) ^1H - ^{13}C heteronuclear correlation spectrum of **apo-1**. (C) ^1H - ^{13}C heteronuclear correlation spectrum of 1-CO_2 .

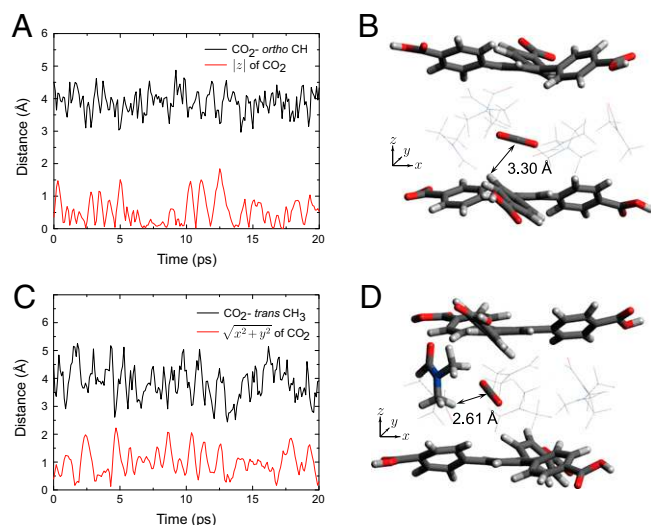


Fig. 4. Fluctuation of minimum distance d between the carbon atom in CO_2 molecule and the *ortho*-CH and the *trans*- CH_3 hydrogen atoms. (A) Comparison of $|z|$ of the CO_2 molecule and d shows that dips in d are correlated with the peaks in $|z|$. (B) A representative snapshot for which d falls below 3.5 Å is shown, where only the H_3BTB units and CO_2 molecule are highlighted. (C) Comparison of $(x^2 + y^2)^{1/2}$ of the CO_2 molecule and d shows that dips in d are correlated with the peaks in $(x^2 + y^2)^{1/2}$. (D) A representative snapshot for which d falls below 3.5 Å is shown, where only the H_3BTB units, CO_2 molecule, and interacting DMF molecule are highlighted.

the CO_2 molecule is correlated with the distance between the carbon atom and the *ortho*-CH groups (Fig. 4 A and B). When the CO_2 molecule hits the cage wall, a DMF molecule can rotate to bring the *trans*- CH_3 groups inward, leading to the NMR coupling signals (Fig. 4 C and D).

More detailed information about the structural incorporation of CO_2 and its motional behavior is obtained from the ^{13}C anisotropic chemical shift (CSA) (49). The CSA of rigid CO_2 is particularly large, 314.5 ppm (50). For isotropic motion the anisotropy is completely averaged. For anisotropic motion, however, the anisotropy is reduced and can be quantified by a dynamic order parameter with $-0.5 \leq S \leq 1$ (51). Rigid incorporation of CO_2 corresponds to $S = 1$, complete isotropic motion to $S = 0$, and axial rotation about a fixed axis perpendicular to the $\text{O}=\text{C}=\text{O}$ symmetry axis leads to $S = -0.5$. The best fit to the experimental spectrum yields $S = -0.36$ (SI Appendix, Fig. S13). The symmetry of the motionally averaged tensor shows that the effective rotation axis about which the jumps occur has at least threefold symmetry. Such a spectrum can result from a rotation about an axis inclined at 72° with the $\text{O}=\text{C}=\text{O}$ symmetry axis (52). The same spectrum (or order parameter), however, is obtained for a rotation perpendicular to the $\text{O}=\text{C}=\text{O}$ symmetry axis with fluctuations of the rotation axis of $\pm 20^\circ$. This dynamics is in good agreement with our DFTB-based MD simulation. The anisotropy information can also be extracted from the MD trajectories. We calculated the angle θ at which the CO_2 is inclined from the horizontal plane at each time step of the MD trajectories. The CO_2 molecule lies horizontally for most of the time, while it shows occasional tumbling motion (Movie S1). According to the plot of θ shown in SI Appendix, Fig. S14, the SD of θ is 25° , consistent with the analysis of chemical shift anisotropy from the NMR study.

Moreover, intrinsically dynamic molecular fluctuation of DMF molecules in crystal **1** can provide routes for the guest molecules to diffuse through the crystal. Indeed, such dynamics of the DMF molecules in **1** is observed by solid-state ^2H NMR (SI Appendix, Fig. S15). The quadrupolar coupling constant of the amide deuteron is calculated to be about 143 kHz, smaller than the value

(154–181 kHz) reported for the rigid amide deuteron in DMF-d_7 (53). Similarly, the quadrupolar coupling constants for methyl deuterons are reduced to ~ 45 kHz, smaller than the typical value (~ 55 kHz) reported for fast threefold rotation of methyl groups in DMF-d_7 (54). This additional reduction of the quadrupolar coupling constant indicates the existence of fast threefold rotation and additional dynamic motion.

The motions of DMF molecules relevant to intercage CO_2 transfer are investigated using density functional theory (DFT) (55, 56). The most stable position for CO_2 is the center of each cage (A and E positions in Fig. 5). The positions B and D are the transition states along the CO_2 pathway from A to E. One of the DMF molecules acts like a gate, and the hydrogen bond between DMF and H_3BTB acts as a hinge of the DMF gate when CO_2 passes by (Movie S2). As the DMF gate opens by rotating it to the outside of the cage A, the CO_2 molecule passes by the carboxyl group of DMF and moves from A to C for which the barrier (B) is 18.6 kcal/mol. At the intermediate state C where the gate is closed and the CO_2 molecule stays between two DMF gates, the energy is 8.9 kcal/mol higher than the starting point A. Then, this CO_2 pushes the gate (one of the DMF molecules in cage E) into cage E and passes by the methyl groups of DMF around D. The barrier for this process from the intermediate point C is 7.2 kcal/mol. The experimental activation energy is about 10.1 kcal/mol (SI Appendix, Table S4), lower than the maximum theoretical barrier height 18.6 kcal/mol. This discrepancy arises from a simplified unit cell including only two cages (due to a very large size DFT calculation), which implies a collective gate opening at every possible pair of cages in the bulk in the DFT simulation. Therefore, the simulated value should be regarded as an upper bound for the real barrier height. The calculation results, although not quantitative, provide very useful qualitative understanding of the gate-opening energy profiles and transition paths.

We have observed the structural dynamics for the reversible CO_2 sorption process in seemingly nonporous ordered cages using in situ XRD and solid-state NMR. Our observation demonstrates that the confinement of gas molecules in the small cages allows the direct visualization of confined gas molecules by single-crystal X-ray crystallography at high temperature even in

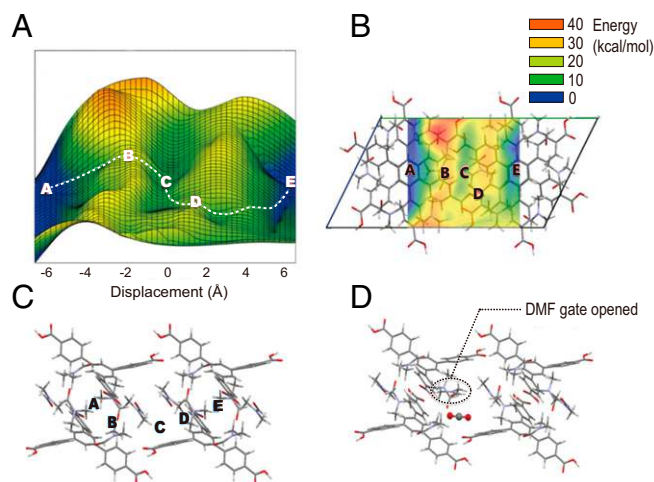


Fig. 5. Pathway and potential energy surface (PES) for translocation of CO_2 between two neighboring cages. (A) Two-dimensional PES in a supercell inside the crystal. The central carbon position of a CO_2 molecule along the lowest energy pathway is marked A to E. (B) Side view of the supercell. (C) Top view of the supercell together with the contour map of PES. (D) Snapshot when a DMF molecular gate is fully opened near the midpoint of B and C so that the CO_2 molecule passes through the wall between cages. See the movie file provided as supporting information (Movie S2).

the absence of strong binding interactions. In general, in most gas storage materials including molecular organic frameworks, gases are more stored at low temperatures. However, in this material gases are able to be stored at high temperatures. This temperature-driven transient-gate controlled gas storage mechanism in ordered cages could open approaches to store small molecules in ordered arrays toward unusual collective properties and to release high-purity nonstorable molecules at high concentration for ready use.

Materials and Methods

General Considerations. H₃BTB was purchased from Tokyo Chemical Industry Co. DMF was purchased from Samchun Chemical Co. Deuterated DMF-d₇ and DMF-d₁ were purchased from Cambridge Isotope Laboratories, Inc. The crystals of **1** were prepared by dissolving excess H₃BTB in minimal DMF solvent in a hot oven. The solution was then slowly cooled down to room temperature, and the crystals formed were collected by filtration and dried in air. For ²H NMR experiments, deuterated crystals were prepared in either DMF-d₇ or DMF-d₁ solvent (Cambridge Isotope Laboratories, Inc.). TGA measurements were carried out at a rate of 10 °C/min over the temperature of 30–550 °C under a nitrogen atmosphere using a thermogravimeter (model TG/DTA 6200, Seiko Instruments).

In Situ Single-Crystal X-Ray Crystallography. In situ single-crystal XRD experiments were performed at the 2D SMC beam line at the Pohang Light Source II (PLS-II), Korea. The ADSC Q210 ADX program (57) was used for data collection, and HKL3000sm (Version 703r) (58) was used for cell refinement, reduction, and absorption correction. In situ variable-pressure single-crystal diffraction data were measured with a custom-made vacuum manifold and goniometer head at PLS-II. The extrahigh purity quality of carbon dioxide gas (DAEHAN Gas Company, 99.999%) was used. Before data collection the crystal was outgassed under a vacuum at 323 K until no significant electron density inside the cage was observed; then, the sample was maintained at 323 K by using Oxford Instrument CryojetHT. The crystal structure was solved by the direct method with SHELX-XS (Version 2013/1) and refined by full-matrix least-squares calculations with the SHELX-XL (Version 2014/7) program package (59). The position of the CO₂ molecule was located at a threefold rotatory inversion symmetry as *R*-3 space group in Fourier difference maps. The occupancy of the atoms in CO₂ was refined to 100%. The CO bond length was restrained to 1.16 Å using DFIX during the least-squares refinement. All nonhydrogen atoms were refined with anisotropic displacement coefficients. The hydrogen atoms were assigned isotropic displacement coefficients $U_{\text{iso}}(\text{H}) = 1.2$ or $1.5U_{\text{eq}}$, and their coordinates were allowed to ride on their respective atoms except oxygen hydrogen of carboxylic acid. A summary of some important crystallographic details can be found in *SI Appendix, Tables S1 and S2*. The supporting crystallographic data for this paper are contained at the Cambridge Crystallographic Data Centre, CCDC-1008184, CCDC-1008185, and CCDC-1008186. These data can be obtained free of charge from the CCDC via www.ccdc.cam.ac.uk/data_request/cif.

In Situ Synchrotron XPRD Analysis. Powder of the crystal **1** was packed in the 0.4-mm diameter (wall thickness, 0.01 mm) capillary (Hampton Research, glass number 50). The diffraction data measured transparency as Debye-Scherrer pattern with the 150-mm sample-to-detector distance in 60-s exposure with synchrotron radiation ($\lambda = 1.20043$ Å) on an ADSC Quantum-210 detector at 2D SMC with a silicon (111) double-crystal monochromator at the PLS-II, Korea. Before data collection, the sample powder was outgassed at 323 K under a vacuum until its X-ray powder pattern showed a pure phase. CO₂ was introduced in the capillary at each step in which the pressure control was used to increase from 1 to 25 bar and to decrease from 25 to 1 bar by using a fine adjustable needle valve, and then the X-ray powder patterns were collected. For 273 and 223 K, the maximum pressures were set to 9 and 5 bar, respectively. The ADX program was used for data collection, and the Fit2D program (60) was used for the integration of 2D to 1D pattern and wavelength, detector distance refinement, and a calibration measurement of a National Institute of Standards and Technology (NIST) Si 640c standard sample.

Solid-State MAS NMR. High-resolution solid-state NMR studies have been performed on the Bruker Avance III console operating at 700.21-MHz ¹H Larmor frequency using a commercial double-resonance MAS probe supporting zirconia rotors of 2.5-mm outer diameter. Heteronuclear correlation spectra of **1** and **1**•CO₂ have been recorded using a Lee–Goldburg cross-polarization suppressing spin diffusion during polarization transfer combined with the frequency-switched Lee–Goldburg decoupling scheme averaging ¹H homonuclear dipolar couplings during ¹H evolution and

thus improving the spectral resolution in the ¹H dimension. The correlation measurements have been performed at ambient conditions and 18-kHz MAS frequency applying rf pulses with 100-kHz rf nutation frequency. A cross polarization contact time of 0.5 ms was chosen for polarization transfer providing at the same time good signal intensities and sufficient selectivity, and the power level on the ¹³C channel was optimized to obtain maximum signal intensities. Phase-sensitive correlation spectra with good signal-to-noise ratios could be recorded with 128 transients for each of the 128 increments in the ¹H dimension using the States method. The chemical shift recoupling experiment using the SUPER NMR technique has been performed on a Bruker Avance II console operating at 300.13-MHz ¹H Larmor frequency using a commercial double-resonance MAS probe for zirconia rotors of 2.5-mm outer diameter at 4,125-Hz MAS frequency. The experimental parameters were chosen and the data processing was done according to the detailed description given in the SUPER NMR paper using the shearing automation provided by BRUKER BioSpin GmbH. Eighty increments for the anisotropic line shape dimension have been recorded with 1,280 transients each.

²H NMR Experiments. ²H NMR experiments were performed on a Varian Unity Inova 600 spectrometer with a 14.1-T wide-bore magnet (Oxford Instruments) corresponding to the deuterium frequency of 92.0968 MHz (Korea Basic Science Institute, Daegu Center). ²H NMR spectra were measured with a solid-state echo pulse sequence using 2.5-μs 90° pulse, 1.5-ms acquisition time, 1-s recycle time, and 10-μs echo delay time.

Theoretical Calculations. The DFTB+ package was used for the MD simulations using the self-consistent-charge DFTB method (47, 48). The crystal **1** was modeled with the three-cage unit cell with an appropriate periodic boundary condition. A Nosé–Hoover thermostat was used to set the simulation temperature to the experimental temperature 323 K. The chain length for the thermostat was three, and the time step was chosen to be 1.0 fs. Five trajectories of 20 ps long were generated, and the snapshots of the system were recorded every 100 steps, i.e., 0.1 ps. A video clip (*Movie S1*) is made from the snapshots of one of the cages. DFT calculations were performed with the projected augmented wave method by using the Vienna Ab initio Simulation Package (VASP) (55) with plane-wave cutoff of 400 eV. Generalized gradient approximation was used with the PW91 and optB88-vdW functionals.

Gas Adsorption Experiments. Gas adsorption experiments were performed with the BELSORP-HP high-pressure gas adsorption measuring system and the BELSORP-Mini low-pressure gas adsorption measuring system (BEL Japan, Inc.) equipped with a temperature control unit. At least 300 mg of sample pretreated at 323 K for more than 12 h was loaded in a sample holder and CO₂, N₂, CH₄, and O₂ high-pressure gas adsorption isotherms were measured by a volumetric method in the range of 0–15 bar at 323 K. The gas non-ideality was corrected using second and third virial coefficients, which were calculated with the gas density data from NIST database (webbook.nist.gov/chemistry/fluid/). The extrahigh purity quality (>99.99%) of gases was used for all adsorption measurements. IAST selectivity calculations were performed using experimentally measured isotherms. The parameters for selectivity calculations were obtained by fitting the adsorption isotherms using the single-site Langmuir–Freundlich (for N₂ and O₂) (40) and the single-site Langmuir model (for CO₂ and CH₄) (40). Adsorption kinetics were measured at 298, 313, and 323 K, using the “adsorption rate measurement” option in the BELSORP-HP operation software. The adsorption kinetic data were analyzed with the BELDyna software provided from BEL Japan, Inc. The rate constants (*k*) were determined by fitting of $(C - C_{\text{eq}})/(C_{0\text{n}} - C_{\text{eq}})$ vs. time graph and then the activation energy (*E_a*) was calculated by plotting $\ln(k)$ vs. $1/T$, in which the slope of the line corresponds to $-E_{\text{a}}/R$.

Breakthrough Experiments. The samples were initially activated at 323 K for 12 h under vacuum. They were packed into the column and then degassed by a He flow of 30 mL/min at 323 K. A stainless steel column with a length of 5 cm and an internal diameter of 0.44 cm was filled with about 372 mg of adsorbent. The remainder of the column was filled with glass wools. The column was placed in a ventilated thermostated oven. Gas flows were regulated with mass flow controllers (Bronkhorst). All of the experiments were carried out at 323 K. The composition of the gas flow at the outlet of the column was measured online by a mass spectrometer (Pfeiffer Vacuum Prisma QME 200). Between each measurement, the adsorbent was typically regenerated in a helium flow (30 mL/min) for at least 10 min. The breakthrough curves were then measured by switching the He flow to a flow containing CO₂/CH₄ mixture (CO₂:CH₄ = 50:50) or CO₂/N₂ mixture (CO₂:N₂ = 15:85). Due to large particle sizes, only a very minor pressure drop ($\Delta P = 0.1$ bar) was observed under the experimental conditions.

ACKNOWLEDGMENTS. This work was supported by National Research Foundation of Korea (National Honor Scientist Program: 2010-0020414) and KISTI (KSC-2014-C3-019, KSC-2014-C3-020). We acknowledge the Pohang Accelerator Laboratory for the use of the synchrotron 2D (SMC) beamline (2014-3rd-2D-004 and 2015-1st-2D-003). Experiments

at the Pohang Light Source were supported in part by Ministry of Science, ICT and Future Planning of Korea and Pohang University of Science and Technology. We acknowledge the Korea Basic Science Institute Daegu Center for the use of 600-MHz NMR spectrometer for deuterium NMR experiments.

- Phan A, et al. (2010) Synthesis, structure, and carbon dioxide capture properties of zeolitic imidazolate frameworks. *Acc Chem Res* 43(1):58–67.
- Sumida K, et al. (2012) Carbon dioxide capture in metal-organic frameworks. *Chem Rev* 112(2):724–781.
- Hong BH, Bae SC, Lee C-W, Jeong S, Kim KS (2001) Ultrathin single-crystalline silver nanowire arrays formed in an ambient solution phase. *Science* 294(5541):348–351.
- Horike S, Shimomura S, Kitagawa S (2009) Soft porous crystals. *Nat Chem* 1(9):695–704.
- Wu H, Gong Q, Olson DH, Li J (2012) Commensurate adsorption of hydrocarbons and alcohols in microporous metal organic frameworks. *Chem Rev* 112(2):836–868.
- Wang B, Côté AP, Furukawa H, O’Keeffe M, Yaghi OM (2008) Colossal cages in zeolitic imidazolate frameworks as selective carbon dioxide reservoirs. *Nature* 453(7192):207–211.
- Tozawa T, et al. (2009) Porous organic cages. *Nat Mater* 8(12):973–978.
- Atwood JL, Barbour LJ, Jerga A, Schottel BL (2002) Guest transport in a nonporous organic solid via dynamic van der Waals cooperativity. *Science* 298(5595):1000–1002.
- Enright GD, Udachin KA, Moudrakovski IL, Ripseester JA (2003) Thermally programmable gas storage and release in single crystals of an organic van der Waals host. *J Am Chem Soc* 125(33):9896–9897.
- Ananchenko GS, et al. (2006) Guest exchange in single crystals of van der Waals nanocapsules. *Angew Chem Int Ed Engl* 45(10):1585–1588.
- Ananchenko GS, et al. (2007) A molecular turnstile in *para*-octanoyl calix[4]arene nanocapsules. *Chem Commun (Camb)* (7):707–709.
- Ananchenko GS, Moudrakovski IL, Coleman AW, Ripseester JA (2008) A channel-free soft-walled capsular calixarene solid for gas adsorption. *Angew Chem Int Ed Engl* 47(30):5616–5618.
- Thallapally PK, et al. (2008) Gas-induced transformation and expansion of a nonporous organic solid. *Nat Mater* 7(2):146–150.
- Udachin KA, Moudrakovski IL, Enright GD, Ratcliffe CI, Ripseester JA (2008) Loading-dependent structures of CO₂ in the flexible molecular van der Waals host *p*-tert-butylcalix[4]arene with 1 : 1 and 2 : 1 guest-host stoichiometries. *Phys Chem Chem Phys* 10(31):4636–4643.
- Breite MD, Cox JR, Adams JE (2010) Energetics of intercavity diffusion in a simple model of a low-density *p*-tert-butylcalix[4]arene crystal. *J Am Chem Soc* 132(32):10996–10997.
- Tsue H, et al. (2012) Crystallographic analysis of CO₂ sorption state in seemingly nonporous molecular crystal of azacalix[4]arene tetramethyl ether exhibiting highly selective CO₂ uptake. *CrystEngComm* 14(3):1021–1026.
- Herbert SA, Janiak A, Thallapally PK, Atwood JL, Barbour LJ (2014) Diffusion of vapor guests into a seemingly non-porous organic crystal. *Chem Commun (Camb)* 50(98):15509–15512.
- Jacobs T, Smith VJ, Thomas LH, Barbour LJ (2014) Carbon dioxide entrapment in an organic molecular host. *Chem Commun (Camb)* 50(1):85–87.
- Riddle JA, Bollinger JC, Lee D (2005) Escape from a nonporous solid: Mechanically coupled biconcave molecules. *Angew Chem Int Ed Engl* 44(41):6689–6693.
- Burchell TJ, Enright GD, Ripseester JA (2008) Guest capture, storage and removal in the TATM host framework: A single-crystal study. *New J Chem* 32(5):864–871.
- Dobrzańska L, Lloyd GO, Raubenheimer HG, Barbour LJ (2006) Permeability of a seemingly nonporous crystal formed by a discrete metallocyclic complex. *J Am Chem Soc* 128(3):698–699.
- Tian J, Thallapally PK, Dalgarno SJ, Atwood JL (2009) Free transport of water and CO₂ in nonporous hydrophobic clarithromycin form II crystals. *J Am Chem Soc* 131(37):13216–13217.
- Chandler BD, et al. (2008) Mechanical gas capture and release in a network solid via multiple single-crystalline transformations. *Nat Mater* 7(3):229–235.
- Xiao B, et al. (2009) Chemically blockable transformation and ultrasensitive low-pressure gas adsorption in a non-porous metal organic framework. *Nat Chem* 1(4):289–294.
- Bradshaw D, Warren JE, Rosseinsky MJ (2007) Reversible concerted ligand substitution at alternating metal sites in an extended solid. *Science* 315(5814):977–980.
- Kawamichi T, Haneda T, Kawano M, Fujita M (2009) X-ray observation of a transient hemiaminal trapped in a porous network. *Nature* 461(7264):633–635.
- Legrand Y-M, van der Lee A, Barboiu M (2010) Single-crystal X-ray structure of 1,3-dimethylcyclobutadiene by confinement in a crystalline matrix. *Science* 329(5989):299–302.
- Rowell JLC, Spencer EC, Eckert J, Howard JAK, Yaghi OM (2005) Gas adsorption sites in a large-pore metal-organic framework. *Science* 309(5739):1350–1354.
- Vaidhyanathan R, et al. (2010) Direct observation and quantification of CO₂ binding within an amine-functionalized nanoporous solid. *Science* 330(6004):650–653.
- Plonka AM, et al. (2013) Mechanism of carbon dioxide adsorption in a highly selective coordination network supported by direct structural evidence. *Angew Chem Int Ed Engl* 52(6):1692–1695.
- Liao P-Q, et al. (2012) Strong and dynamic CO₂ sorption in a flexible porous framework possessing guest chelating claws. *J Am Chem Soc* 134(42):17380–17383.
- Takamizawa S, et al. (2010) Crystal transformation and host molecular motions in CO₂ adsorption process of a metal benzoate pyrazine (M^(II) = Rh, Cu). *J Am Chem Soc* 132(11):3783–3792.
- Zhang J-P, Chen X-M (2009) Optimized acetylene/carbon dioxide sorption in a dynamic porous crystal. *J Am Chem Soc* 131(15):5516–5521.
- Lin J-B, Xue W, Zhang J-P, Chen X-M (2011) An ionic porous coordination framework exhibiting high CO₂ affinity and CO₂/CH₄ selectivity. *Chem Commun (Camb)* 47(3):926–928.
- Takamizawa S, Takasaki Y, Miyake R (2009) Host-guest transformational correlations for a gas inclusion co-crystal on changing gas pressure and temperature. *Chem Commun (Camb)* (43):6625–6627.
- Jacobs T, et al. (2012) In situ X-ray structural studies of a flexible host responding to incremental gas loading. *Angew Chem Int Ed Engl* 51(20):4913–4916.
- Spek AL (2009) Structure validation in chemical crystallography. *Acta Crystallogr D Biol Crystallogr* 65(Pt 2):148–155.
- Kim KS, Tarakeswar P, Lee JY (2000) Molecular clusters of π -systems: Theoretical studies of structures, spectra, and origin of interaction energies. *Chem Rev* 100(11):4145–4186.
- Myers AL, Prausnitz JM (1965) Thermodynamics of mixed-gas adsorption. *AIChE J* 11(1):121–127.
- Mason JA, Sumida K, Herm ZR, Krishna R, Long JR (2011) Evaluating metal-organic frameworks for post-combustion carbon dioxide capture via temperature swing adsorption. *Energy Environ Sci* 4(8):3030–3040.
- Sircar S (2006) Basic needs for design of adsorptive gas separation processes. *Ind Eng Chem Res* 45(16):5435–5448.
- Na K, et al. (2011) Directing zeolite structures into hierarchically nanoporous architectures. *Science* 333(6040):328–332.
- Loiseau T, et al. (2004) A rationale for the large breathing of the porous aluminum terephthalate (MIL-53) upon hydration. *Chemistry* 10(6):1373–1382.
- Rossum B-J, Förster H, de Groot HJM (1997) High-field and high-speed CP-MAS ¹³C NMR heteronuclear dipolar-correlation spectroscopy of solids with frequency-switched Lee-Goldburg homonuclear decoupling. *J Magn Reson* 124(2):516–519.
- Ladizhansky V, Vega S (2000) Polarization transfer dynamics in Lee-Goldburg cross polarization nuclear magnetic resonance experiments on rotating solids. *J Chem Phys* 112(16):7158–7168.
- Fung BM, Khitrin AK, Ermolaev K (2000) An improved broadband decoupling sequence for liquid crystals and solids. *J Magn Reson* 142(1):97–101.
- Aradi B, Hourahine B, Frauenheim T (2007) DFTB+, a sparse matrix-based implementation of the DFTB method. *J Phys Chem A* 111(26):5678–5684.
- Elstner M, et al. (1998) Self-consistent-charge density-functional tight-binding method for simulations of complex materials properties. *Phys Rev B* 58(11):7260–7268.
- Liu S-F, Mao J-D, Schmidt-Rohr K (2002) A robust technique for two-dimensional separation of undistorted chemical-shift anisotropy powder patterns in magic-angle-spinning NMR. *J Magn Reson* 155(1):15–28.
- Bowers CR, Long HW, Pietrass T, Gaede HC, Pines A (1993) Cross polarization from laser-polarized solid xenon to ¹³CO₂ by low-field thermal mixing. *Chem Phys Lett* 205(2-3):168–170.
- Hansen MR, Graf R, Spiess HW (2013) Solid-state NMR in macromolecular systems: Insights on how molecular entities move. *Acc Chem Res* 46(9):1996–2007.
- Kong X, et al. (2012) CO₂ dynamics in a metal-organic framework with open metal sites. *J Am Chem Soc* 134(35):14341–14344.
- Balakrishnan NS (1989) NMR determination of quadrupole coupling constants of deuterons in N,N-dimethylformamide-d₇. *J Magn Reson* 83(1):233–245.
- Wann M-H, Harbison GS (1994) Axial asymmetry in the nuclear magnetic resonance spectra of deuterated methyl groups: An alternative explanation. *J Chem Phys* 101(1):231–237.
- Kresse G, Furthmüller J (1996) Efficient iterative schemes for ab initio total-energy calculations using a plane-wave basis set. *Phys Rev B Condens Matter* 54(16):11169–11186.
- Klimeš J, Bowler DR, Michaelides A (2011) van der Waals density functionals applied to solids. *Phys Rev B* 83(19):195131–195131-13.
- Arvai AJ, Nielsen C (1983) ADSC Quantum-210 ADX Program (Area Detector System Corporation, Poway, CA).
- Otwinowski Z, Minor W (1997) Processing of X-ray diffraction data collected in oscillation mode. *Methods in Enzymology*, eds Carter CW Jr, Sweet RM (Academic, New York), Vol 276, Part A, pp 307–326.
- Sheldrick GM (1997) SHELXTL-PLUS, Crystal Structure Analysis Package (Bruker Analytical X-ray, Madison, WI).
- Hammersley A (2014) Fit2D program. (Version 16.041).